Catalysis Today 397-399 (2022) 16–27

Contents lists available at ScienceDirect

Catalysis Today

journal homepage: www.elsevier.com/locate/cattod

Solvothermal synthesis of ZnO spheres: Tuning the structure and morphology from nano- to micro-meter range and its impact on their photocatalytic activity

Zoltán Kovács [a,b,c], Csanád Molnár [a], Tamás Gyulavári [a,c], Klára Magyari [c,d], Zsejke-Réka Tóth [c,d], Lucian Baia [b,d,*], Zsolt Pap [c,d,e,**], Klara Hernádi [a,c,f,***]

[a] Research Group of Environmental Chemistry, Institute of Chemistry, University of Szeged, Tisza Lajos krt. 103, HU-6720 Szeged, Hungary
[b] Faculty of Physics, Babeș-Bolyai University, Str. Mihail Kogălniceanu 1, RO-400084 Cluj-Napoca, Romania
[c] Department of Applied and Environmental Chemistry, University of Szeged, Rerrich tér 1, HU-6720 Szeged, Hungary
[d] Centre of Nanostructured Materials and Bio-Nano Interfaces, Institute for Interdisciplinary Research on Bio-Nano-Sciences, Treboniu Laurian 42, RO-400271 Cluj-Napoca, Romania
[e] Institute for Research, Development and Innovation in Applied Natural Sciences, Fântânele Street Nr. 30, RO-400327 Cluj-Napoca, Romania
[f] Institute of Physical Metallurgy, Metal Forming and Nanotechnology, University of Miskolc, HU-3515 Miskolc-Egyetemváros, Hungary

ARTICLE INFO

Keywords:
ZnO
Spherical morphology, phenol
Hierarchical particles
Photocatalysis

ABSTRACT

Nano- and micro-sized ZnO spheres were fabricated via a simple solvothermal synthesis using two different precursors, while diethanolamine was used to control the morphology. The applied solvent composition, precursor ratio and solvothermal treatment temperature were mathematically correlated with the diameter of spheres. The crystallite size could be easily controlled by adjusting the temperature, providing flexibility during synthesis. The photocatalytic activity and its dependence on the unique morphology were investigated via the decomposition of phenol model pollutant. It was revealed that the surface proprieties were more defining than the secondary particle size in this regard. A surprising synergic effect was observed between the ratio of exposed crystallographic planes of (100) and (002) and crystallite size upon the activity, while the size of the spheres shows little influence. The presented method enables the flexible design of ZnO photocatalysts with spherical morphology in a tunable size range.

1. Introduction

Many methods have addressed the problem of wastewater treatment. However, clean water is still not a universal commodity and the developing pharmaceutical and chemical industries are constantly increasing the list of pollutants present in wastewaters. Thus, there is a constant need for alternative techniques with general applicability, which are less dependent on the chemical nature of water-soluble pollutants. This difficult issue gave rise to a huge number of publications in the field of photocatalysis as a promising candidate, due to its potential to be used as a non-selective oxidation process. ZnO remains to be one of the most promising semiconductors for photocatalysis due to its high UV absorption, and because it is widely available, cheap and non-toxic. Numerous attempts have already been made to improve its photocatalytic efficiency via the following methods: structural modification [1], doping with various elements [2], functionalizing the surface with different compounds [3], preparing composites with other semiconductors (e.g., TiO_2 [4], AgBr [5], WO_3 [6], CeO_2 [7], BiOBr [8], CuO [9], reduced graphene-oxide [10], carbon nanotubes [11]) or with noble metals [12] and controlling its morphology [10,13,14].

Over the last few decades, the preparation of semiconductors with various morphologies has become a common practice to tune the structural, thermal, electric, optical, and photoelectric proprieties [13]. For ZnO, the following geometries have already been synthesized: prisms [15], rods [16], needles [17], urchins [14], disks [18], tetrapods [19], spheres [4,20] and hollow structures [20–23]. Different

* Corresponding author at: Faculty of Physics, Babeș-Bolyai University, Str. Mihail Kogălniceanu 1, RO-400084 Cluj-Napoca, Romania.
** Corresponding author at: Department of Applied and Environmental Chemistry, University of Szeged, Rerrich tér 1, HU-6720 Szeged, Hungary.
*** Corresponding author at: Research Group of Environmental Chemistry, Institute of Chemistry, University of Szeged, Tisza Lajos krt. 103, HU-6720 Szeged, Hungary.
E-mail addresses: lucian.baia@ubbcluj.ro (L. Baia), pzsolt@chem.u-szeged.hu (Z. Pap), hernadi@chem.u-szeged.hu (K. Hernádi).

https://doi.org/10.1016/j.cattod.2022.03.004
Received 1 April 2021; Received in revised form 18 February 2022; Accepted 2 March 2022
Available online 4 March 2022

morphologies, other than being aesthetic, can greatly redefine the surface structure (e.g., expose dominant crystal facets [24] and provide more defects such as oxygen or zinc vacancies [25,26]), which in turn modifies the optical and ultimately the photocatalytic proprieties of a semiconductor. Even though "simple geometrical" designs have increased the photocatalytic efficiency of ZnO in numerous instances, the arising difficulties during preparation tend to limit the achievable performance. In most cases the microstructure of the particles could only be influenced to a limited extent [27,28]. As a result, this also limits the range of applicability in different advanced oxidation processes.

Although there are some publications in the literature where a specific morphology was successfully controlled in a wide particle size range, such as in the publication of S. Gobboet et al. In their publication the length of ZnO rods were controlled through varying the synthesis parameters; however, such attempts are scarce [29]. In this study, we present a versatile solvothermal method to synthesize ZnO photocatalysts with size-tuneable spherical morphology with average diameters ranging from a few hundred nanometres to several micrometres. The spherical morphology, dispersity and the crystalline structural features were fine-tuned through simple parameter optimization. The photocatalytic activity was measured using phenol as model polutant under UV-A irradiation. Due to the simple spherical morphology, a straightforward mathematical description was provided considering the photocatalytic activity and morphology of the samples.

2. Materials and methods

2.1. Reagents and materials

The materials used in our experiments are zinc acetylacetonate monohydrate ($ZnAA_2$, $Zn(C_5H_7O_2)_2{\bullet}H_2O$, > 99%, Alfa Aesar) and zinc acetate dihydrate ($ZnAc_2$, $Zn(C_2H_3O_2)_2{\bullet}2H_2O$, > 99%, Alfa Aesar) as precursors; absolute ethanol (EtOH, 99.99%, Molar Chemicals) and ultrafiltered water (MQ, conductivity 65,9 μS/cm) as solvents and diethanolamine (DEA, $C_4H_{11}NO_2$, 99.95%, Alfa Aesar) to obtain the spherical morphology. As model pollutant phenol (Spektrum 3D; analytical grade) was used to investigate the photocatalytic activity.

2.2. Synthesis of ZnO

Considering the research published by A. Šarić et al. [30] and A. Gómez-Núñez et al. [31], two synthesis strategies were applied: first, to optimize solvent composition to prepare ZnO photocatalysts with spherical morphology; second, to control various aspects of the morphology (mean diameter, primary particle size).

In each of the experiments a solution of Zn precursor or precursors and DEA was prepared in ethanol-water mixture according to 68 mM total Zn precursor and 204 mM DEA concentration as follows: The Zn precursor were dissolved in corresponding amount of absolute ethanol under continuous stirring for 40 min, then DEA was added in 1:3 molar ratio of Zn to DEA and further stirred for 20 min. The water content was adjusted with MQ water to obtain a certain ethanol-water mixture (ethanol concentration of 80, 90, 95, 99 and 100 v/v%), after which the solution was stirred continuously for another 30 min. This was followed by the transfer of the reaction mixture into a Teflon lined autoclave ($V_{fill}/V_{tot} = 70\%$), which was subjected to a solvothermal treatment at a temperature of 150 °C for 10 h, with a heating rate of 2 °C•min^{-1}. A schematic representation of the synthesis is presented in Fig. 1. The as-prepared ZnOs were washed 3 times with absolute ethanol and once with a 66–33% ethanol/water solution to purify them from the remaining DEA, then dried at 100 °C for 12 h. Every synthesis was carried out in triplicate using 3 autoclaves with internal volumes of 150, 200 and 280 mL.

Based on the synthesis procedure mentioned above, the optimal solvent composition was selected that resulted in the best photocatalytic activity and spherical morphology. Then, the effect of various Zn precursor compositions was investigated ($ZnAc_2$:$ZnAA_2$ = 0:100, 5:95, 10:90, 15:85, 20:80, 25:75, 50: 50, 75:25, 100:0 n/n%) together with the temperature of the solvothermal treatment (120, 150 and 180 °C). The 68 mM cumulative concentration of the Zn precursors were constant throughout all experiments. Sample notation was the following: samples synthesized with pure precursors, $ZnAc_2$ and $ZnAA_2$, were named NS (nanospheres) and MS (microspheres), respectively in cases of the precursor mixtures M"percentage of $ZnAc_2$"NS followed by three digits corresponding to the applied solvothermal temperature (example: ZnO synthesized from $ZnAA_2$ at 150 °C is NS150, from a mixture 5% $ZnAc_2$ and 95% $ZnAA_2$ at 180 °C is M5NS180).

2.3. Characterization

A Rigaku Miniflex II diffractometer was used for X-ray diffractometry measurements (XRD, Shimadzu 6000) applying Cu-Kα radiation (λ_X = 1.5406 Å) and a graphite monochromator. The measurements were carried out between 20 and 80 (2θ°) in 0.02° steps at a 0.5°•min^{-1} scan speed. Crystallite sizes were estimated by 3 different methods: the Scherrer equation, Williamson–Hall analysis [32] and the size strain plot (SSP) [33], taking into account the observations made by R. Yogamalar [34]. Each diffraction peak was fitted with the pseudo-Voigt function in

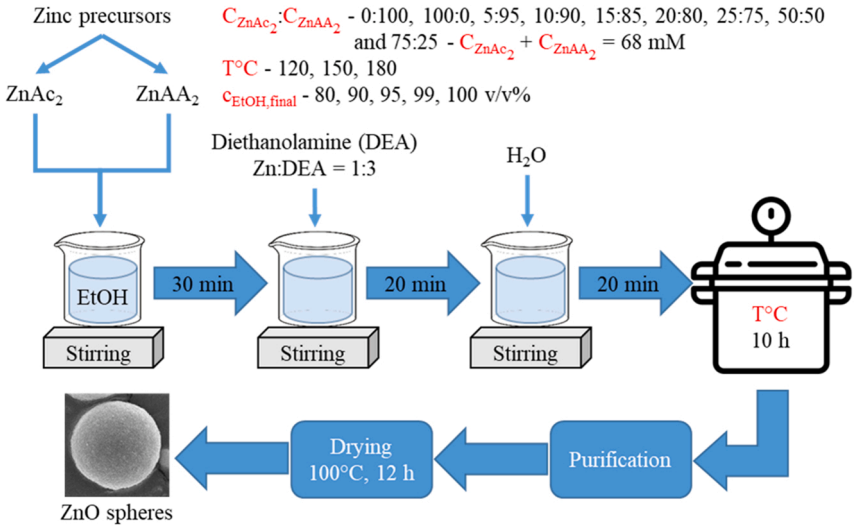

Fig. 1. Schematic representation of the synthesis of spherical ZnO.

OriginPro 2017. The following equations were used:

i) Correction for instrumental broadening:

$$\beta_{hkl} = \left[(\beta_{hkl})^2_{measured} - (\beta_{hkl})^2_{instrumental}\right]^{\frac{1}{2}} \quad (1)$$

ii) Scherrer formula:

$$D = \frac{K \times \lambda_x}{\beta_{hkl} \times cos\theta} \quad (2)$$

iii) W–H equation:

$$\beta_{hkl} \times cos\theta = \frac{K \times \lambda_x}{D} + 4 \times \varepsilon \times sin\theta \quad (3)$$

iv) Size-strain equation:

$$(d_{hkl} \times \beta_{hkl} \times cos\theta)^2 = \frac{K}{D} \times \left(d_{hkl}{}^2 \times \beta_{hkl} \times cos\theta\right) + \left(\frac{\varepsilon}{2}\right)^2 \quad (4)$$

where β_{hkl} is the full width at half maximum, θ is the Bragg angle, d is the distance between adjacent planes represented by the Miller indices (hkl) (calculated from the Bragg equation, i.e., $\lambda = 2d \sin\theta$), D is the crystallite size, K is the shape factor (0.9), and ε represents the crystal strain.

The diffuse reflectance spectra (DRS) of the samples were obtained using a Jasco-V650 UV–vis spectrometer with an integration sphere (ILV-724) in the wavelength range of 250–800 nm using $BaSO_4$ as the reference standard. The band-gap energies were calculated by the Kubelka Munk equation and the Tauc plot representation. Possible electron transitions were estimated from the first derivatives of the DRS.

Fourier transform infrared spectroscopy (FT-IR) measurements were carried out with a JASCO 6200 spectrometer in the 400–4000 cm^{-1} range applying 4 cm^{-1} spectral resolution, using the well-known KBr pellet technique.

The specific surface area of the samples was determined with a BELCAT-A device via N_2 adsorption at 77 K using the Brunauer–Emmett–Teller (BET) approach.

The morphology was analyzed by a Hitachi S-4700 Type II scanning electron microscope (SEM) and a FEI TECNAI G2 20 X-Twin type transmission electron microscope (TEM). The micrographs were further investigated to determine the diameters and their distribution with ImageJ software.

2.4. Assessment of photocatalytic activity

The photocatalytic efficiency of the ZnO samples was evaluated by the decomposition of phenol ($C_{0,phenol} = 0.3$ mM) in aqueous solutions under UV irradiation (6 × 6 W fluorescent lamps, $\lambda_{max} \approx 365$ nm), the irradiation time was 1 h. For a typical experiment, 100 mL of the model compound solution was prepared to which the catalyst was added to set the concentration to 1 $g \cdot L^{-1}$. This was followed by the sonication of the mixture in the dark for 20 min to reach adsorption-desorption equilibrium. During the photocatalytic experiments, the temperature was kept at 25 °C, the homogeneity was assured by constant magnetic stirring at 400 rpm, and the oxygen concentration was maintained by providing constant air supply (30 $L \cdot h^{-1}$) during the measurements.

The phenol concentration was investigated by high performance liquid chromatography (HPLC) with a device consisting of a Merck Hitachi L-7100 low-pressure gradient pump and a Merck-Hitachi L-4250 UV–Vis detector ($\lambda_{detection} = 210$ nm), using a 50–50% methanol/water mixture as the eluent.

3. Results and discussion

3.1. Preliminary investigation of synthesis parameters

The first step was to investigate the morphology and photoactivity of the obtained samples to decide which synthesis conditions will be further exploited. The micrographs (Fig. 2a. and b.) reveal that spherical morphology formed only, when 99% and 100% ethanol concentration was applied, but notable photocatalytic activity was achieved in the first case (Fig. 2c.). Theoretical calculations of A. Šarić et al. [30] and of A. Gómez-Núñez [31] proved that monoethanolamine and triethanolamine could facilitate the formation of relatively stable zinc-based complexes with the two precursors. This was attributed to the ability of the amine and hydroxyl groups to coordinate with the Zn^{2+} ion with the free electron pairs of the N and O atoms. The high flexibility of the ethanolic groups and the similarities between the two alkanolamine allow to assume the formation of similarly stable complexes in the case of diethanolamine. X. Wang et al. found that the increase of monoethanolamine concentration during the synthesis of ZnO photocatalysts leads to an increased number of spherical particles through precipitation from water-based solutions [35]. Moreover, the publication of A. Šarić et al. [36] proved that carrying out the synthesis under similar conditions in organic solvents, the use of triethanolamine in higher concentration resulted also in the formation of more spherical ZnO particles. These two publications provided a good basis to our present work, that is, to investigate the possible relationship between the spherical morphology and photocatalytic activity. The formation of ZnO from these materials requires a hydrolysis step followed by a dehydration process [37,38]. Even though both precursors contain water, for an overall hydroxide formation without its further addition (considering the hydration of the anions too), still, there is a deficit of 50% of water. This could lead to unreacted non-active DEA complexes at the particle boundaries, which could be detrimental to the photocatalytic activity of the surface. Only in high ethanol concentration can the formation of spheres be explained by the DEA acting as a surfactant or by the hydrogen bonding capacity of the adsorbed DEA at the particle boundary.

The effect of solvent composition upon the structure of as-synthesized ZnO was studied by XRD. On the diffractograms of the samples the crystallographic planes of the hexagonal wurtzite structure (100), (002), (101), (102), (110), (103), (200), (112) and (201) (Fig. 3.) were present (JCPDS 36–1451). In addition, with water concentration below 99 v/v%, the appearance of small peaks corresponding to Zn $(OH)_2$ (JCPDS 38-0356) [33,39] were observed. The presence of Zn $(OH)_2$ indicate that the crystallization of ZnO involved a hydroxide formation. In consequence the high water content in the solvent could inhibit the dehydration of $Zn(OH)_2$ at the particle boundary, which could significantly decrease the photocatalytic activity. At 100 v/v% ethanol (without the addition of water) the diffraction peaks are much broader than any of the other samples. This implied poor crystallinity, which could be caused by the slow crystal formation due to the insufficient water to hydrolyze the zinc precursor-DEA complexes. Thus, in further experiments, the solvent composition was chosen to be 99–1% ethanol-water, because at this concentration the spherical morphology was formed, there was no observable $Zn(OH)_2$ impurities and the highest photocatalytic activity was measured.

3.2. Characterization of ZnO spheres

After identifying the main synthesis conditions that are significant for the formation of spherical morphology, various ZnO spheres were obtained applying numerous precursor mixture compositions at 120, 150, 180 °C. These were further studied with XRD, SEM, TEM, IR, and DRS as the effect of temperature and the anion (acetate, acetylacetonate) of the precursor influence the morphology and the structural characteristics.

The XRD patterns of all the ZnO spheres show only peaks

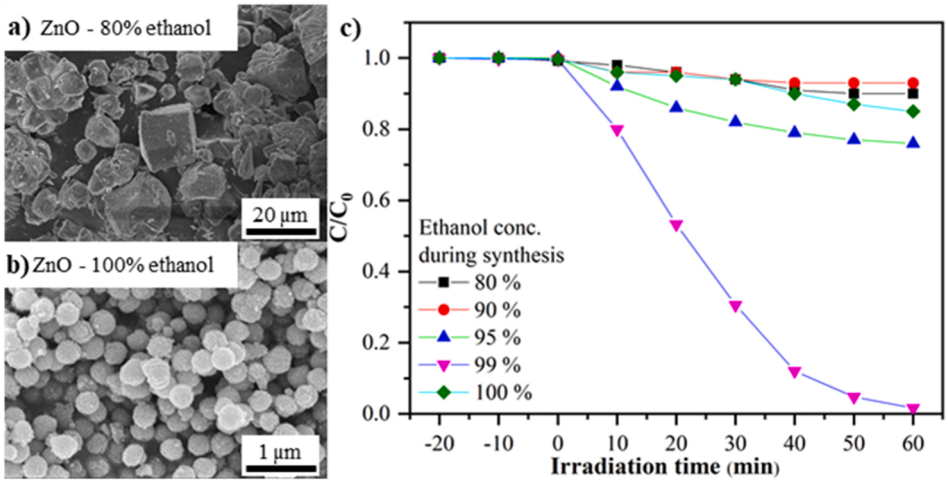

Fig. 2. SEM micrographs (a, b) and phenol degradation curves of the ZnO samples from the preoptimization experiments (c).

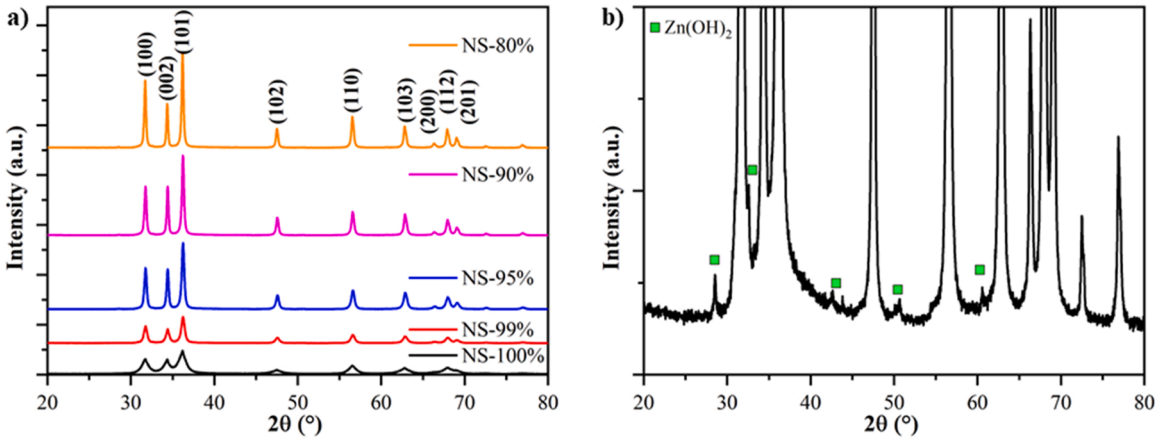

Fig. 3. X-ray diffractograms of ZnO samples synthesized using different ethanol-water solvent compositions with the identified peaks corresponding to the hexagonal ZnO crystal structure (a), and the magnified diffractogram of NS-80% with small peaks corresponding to $Zn(OH)_2$ structure.

corresponding to the hexagonal wurtzite structure with good crystallinity (Fig. 4a.); with no impurity phases. These results were adequate for further mathematical operations. The Scherrer, W-H and SSP methods have various other forms with different terms (e.g., correction terms for anisotropic strain) [40], but in numerous situations they were proved to be unnecessary, as they did not change the results significantly. In the present case, for almost every sample the W-H and SSP methods provide significantly higher values compared to the Scherrer method, because the latter does not take into consideration the strain- and diffraction angle-related issues [32,34].

Table 1. shows the results of these numerical calculations for 2 samples (the rest of the values for the other ZnOs are presented in the

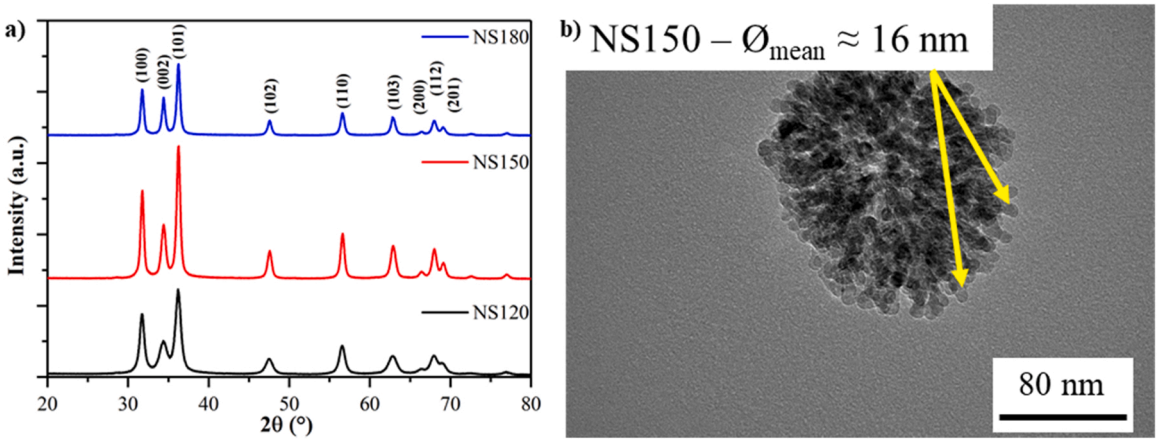

Fig. 4. XRD patterns of ZnO samples synthesized using $ZnAA_2$ precursor at different temperatures (a), and a corresponding TEM micrograph showing crystallites with a mean diameter of 14 nm that build up the sphere (b).

Table 1
Crystallite mean size of NS150, M10NS120 determined by different XRD data evaluation methods.

Sample	Crystallite size (nm)			
	Scherrer	W-H	SSP	TEM
NS150	14.8	16.5	15.0	16
M5NS120	9.6	9.7	7.7	11

supplementary material; Table 1S.). TEM measurements were also carried out to determine if the spheres were solid, without cavity. Moreover, higher magnifications provide the possibility to evaluate the distribution of the small crystals that build up the spheres. The used assessment methods, which are based on the XRD data, generally give information about the average coherent diffraction length of the crystal structure that is usually not consistent with the actual mean crystallite size. Additionally, any imperfection (dislocations, vacancies, interstitial doping, etc.) can induce important size alterations. Such observations were reported by Zak et al. [33], who determined that the actual mean diameter of their observed crystallites by TEM was double to that of the mean size determined by the three methods mentioned above.

To our surprise, the average diameter of the crystallites determined based on the TEM micrographs (Fig. 4b.) resulted in a very similar value compared to the one calculated by the W-H analysis (Table 1.). This result further strenghten that this method approximates the crystallite mean size more efficiently, when the sample is highly crystalline. The TEM micrograph also revealed that the spheres were built from relatively small crystallites. These calculations were performed for all of the ZnO spheres and the values (obtained by the W-H method) are presented in Fig. 5. Irrespective of the temperature applied during the solvothermal treatment, applying mixed precursors always resulted in a lower crystallite mean size compared to that obtained by using pure precursors. Surprisingly, the different mixtures mildly affected the crystallite size, most probably because the liberated acetate ion or acetic acid from the $ZnAc_2$-DEA complex could catalyze the hydrolysis of $ZnAA_2$. Therefore, seed formation could be promoted, as this precursor can hydrolyze in acidic conditions more rapidly. This trend was valid at all temperatures, while regardless of the applied precursor the crystallite size was increasing with temperature.

The abovementioned structural and morphological features (Fig. 5.) imply that the presented method provided valuable information regarding the mean crystallite size and average diameter of the spheres. The tuning of the mean crystallite size seems possible, by simply adjusting the temperature of the solvothermal treatment and the ratio of precursors. Examining the diffractograms further (Fig. 6.), the intensity ratio of the two peaks corresponding to the (002) and (100) crystallographic planes was increased for the samples with the increase of the synthesis temperature. In X-ray diffractometry the variation of the peak intensities could be the consequence of the preferential orientation of the crystallites. In powder diffraction is assumed that the crystallites are randomly oriented. In consequence preferential orientation should not occur. Nonetheless, there are some possibilities for certain geometries of the crystals (e.g. bars, plates) to be arranged preferentially in a flat sample holder along a flat facet with increased size [41]. Considering that ZnO crystallites are arranged in spherical aggregates the possibility of preferential orientation can be eliminated. Besides the change in intensity of the (002) peak, an increase of the FWHM is also observable. The FWHM is directly correlated to the mean crystallite size of the particle by the Scherrer equation [42]. Also, the method assumes that the crystallites are isotropic in all directions. Even though for the application of the Scherrer equation is recommended to use the peak with highest intensity, the calculations were repeated for the other two main diffraction peaks, (100) and (101) (Table S2.). The results show that the crystallite size is always smaller for the (002) peak. Also, the same trend was observed with the ratio of the sizes calculated for (100) and (002) peaks as with the intensity ratios. Consequently, size anisotropy is the cause for the variation in the intensity ratio of (002)/(100), more specifically the decreased crystallite size in the direction normal to (002) plane. The effect of the $I_{(002)}/I_{(100)}$ ratio on the properties of the as-prepared ZnO samples was further discussed in later sections.

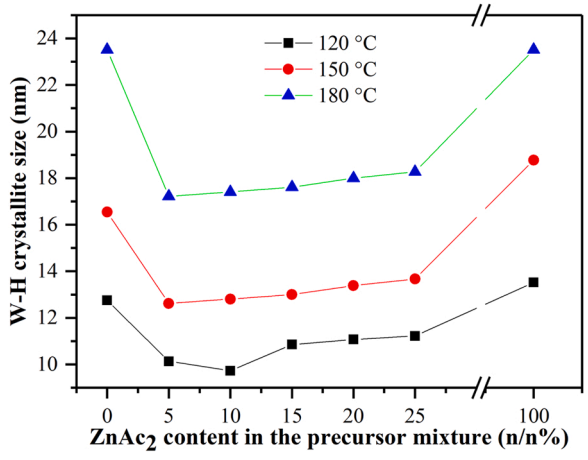

Fig. 5. Crystallite mean size of the synthesized ZnO spheres estimated by the W-H method.

Irrespective of the temperature or precursor type, the as-prepared ZnO samples always showed spherical morphology (Fig. 7.). Based on the experiments performed by using the two precursors purely (i.e., without mixing them), the size of the spheres was of two different order of magnitudes: the size of spheres was of 305 nm for $ZnAA_2$ (NS180) and 2.81 μm for $ZnAc_2$ (MS180). It was inferred that the $ZnAc_2$-DEA_x complexes were less stable and promptly interact with water molecules due to the polarity difference between the acetate ion and acetylacetonate. The formation of hydroxide taking place at a much faster pace could explain the almost tenfold increase of the average diameter of NS180 compared to that of MS180. The diameter distribution histogram for sample NS180 is presented in Fig. S1. The other main difference between the two samples was that the microspheres (MS180) were highly polydisperse, while the nanospheres (NS180) were monodisperse. This arises from the interaction between the byproducts that form due to the hydrolysis of precursors. Acetylacetone is miscible with the solvent, while acetate could be released in an ionic form before becoming protonated, increasing the number of inhomogeneous regions in the sol.

In the experiments, where the precursors were mixed in different ratios, a combination of the individual trends of the previous samples was observed. The mean diameter of these samples was changing according to the zinc-acetate:zinc-acetylacetonate ratio and were situated in the size range between the samples prepared from the pure precursors. This suggests that the two crystallization processes can function in synergy. The size distribution of the spheres decreased significantly to a comparable level with the initial NS180 sample. One exception was identified; the average diameter of M5NS180 (ZnO synthesized by using 5% $ZnAc_2$, 95% $ZnAA_2$) decreased to 155 nm. A linear equation was fitted for the samples synthesized at 180 °C, with a $R^2 > 98\%$. It was concluded that there is a quantifiable relationship between the applied precursor mixture and the resulting mean diameter (Fig. 8a.). These experiments were also carried out at 120 and 150 °C. Completely the opposite trend was observed for the two precursors in relation with temperature. The average diameter increases in the MS samples, while it dramatically decreases in the NS samples in the 120–180 °C range. This surprising difference suggested that the rate determining step for the formation of spherical particles was the aggregation of smaller crystallites. This was because the crystallite mean size is only mildly dependent on the composition of the precursor mixture. Consequently, the cause of the formation of spheres, thus their size was not related to the crystallization reaction directly; rather it seems to be a secondary process.

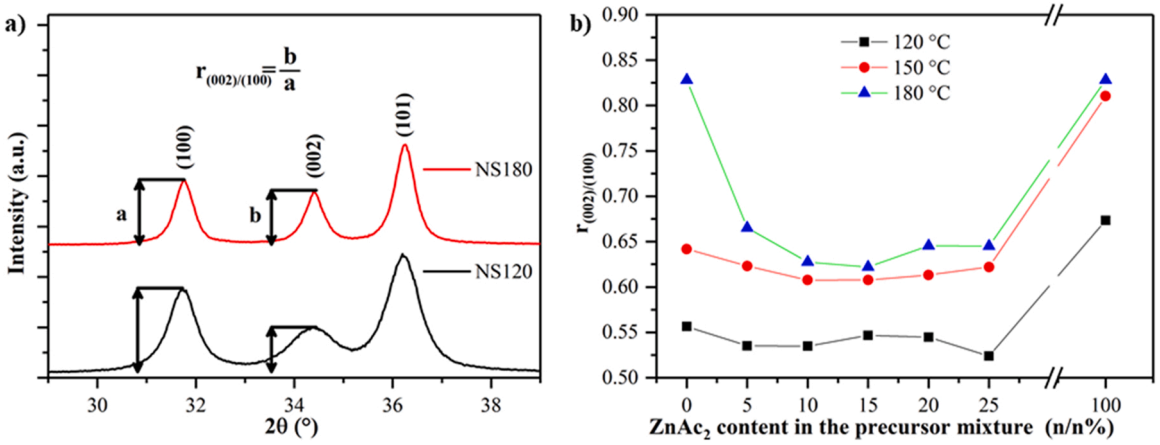

Fig. 6. Ratio of intensities of two peaks corresponding to the (002) and (100) crystallographic planes for some representative samples (a), and the ratio of (002) and (100) intensities as function of the $ZnAc_2$ content in the precursor mixture (b).

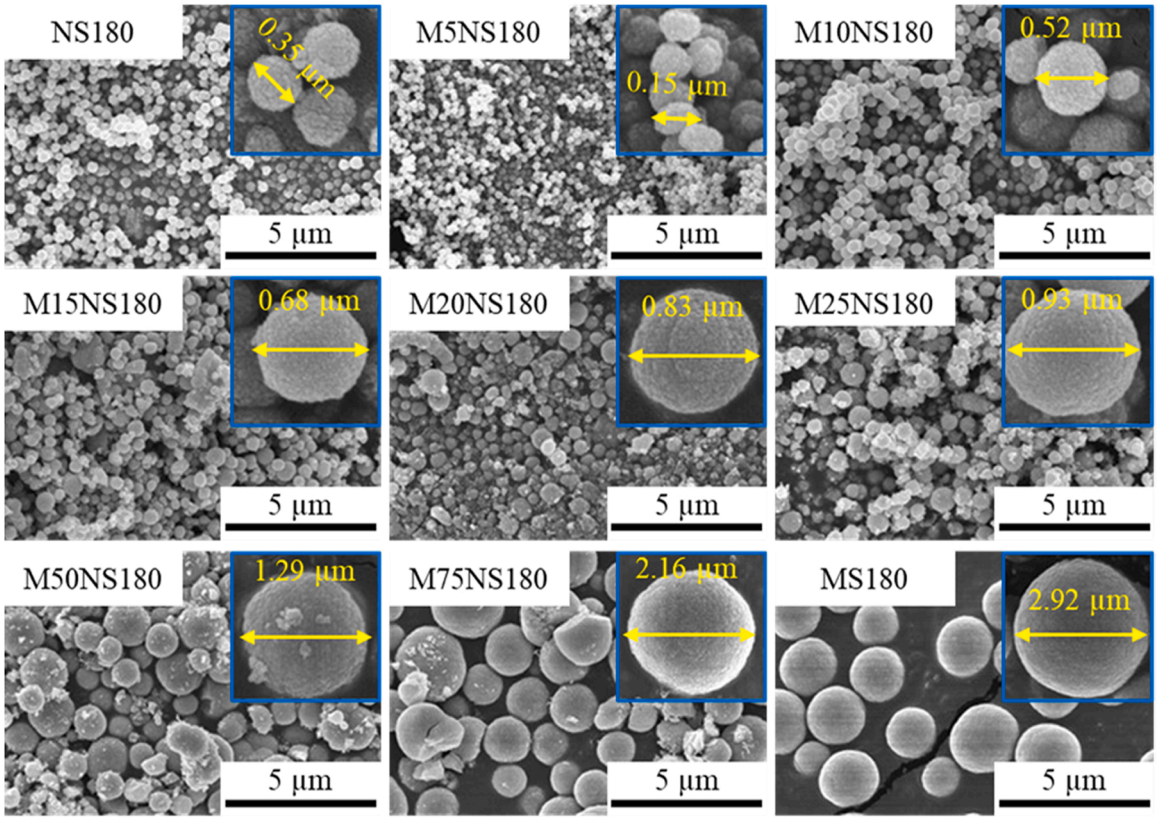

Fig. 7. SEM micrographs of the samples synthesized by applying different precursor mixtures at 180 °C (the ratio of precursors is indicated at the top left corner NS and MS samples with pure $ZnAA_2$, respectively $ZnAc_2$; MxNS180 – the "x" number denotes the molar percentage of $ZnAc_2$ in the $ZnAA_2$-$ZnAc_2$ mixture): NS180, M5NS180, M10NS180, M15NS180, M20NS180, M25NS180, M50NS180, M75NS180 and MS180.

If the average diameter was represented as a function of $ZnAc_2$ content for all three synthesis temperatures (Fig. 8a), one can observe that the overall dependency between them does not change in most cases, only the magnitude of the effect. It is already known that the solvothermal synthesis of ZnO from these precursors is a strongly temperature-driven process. This is due to the hydrolyzation-dehydration process mentioned before, but consequently the same samples synthesized at different temperature follow the same trend. In the present case, examining the mixture precursor series for the three temperatures individually, linear fitting was always successful (with $R^2 > 98\%$). For the fitting only the MS and MNS (precursor mixture samples) series were used, because the majority of deviation was caused by the NS samples. Representing the three set of samples together in Fig. 8a., it can be observed that the temperature becomes a significant factor regarding the size of the spheres as the concentration of $ZnAc_2$ exceeds 25%, because it follows the trend observed for MS. However, below 20% $ZnAc_2$ content the trend corresponds with the NS samples. Normally, it could be expected that this type of relations tilted the trend symmetrically to the middle. However, this is only the case if we assume that the two crystallization processes take part in the overall synergic effect equally. This means that the released acetic acid contributes to the final size of the spheres to a greater extent, compared to that for

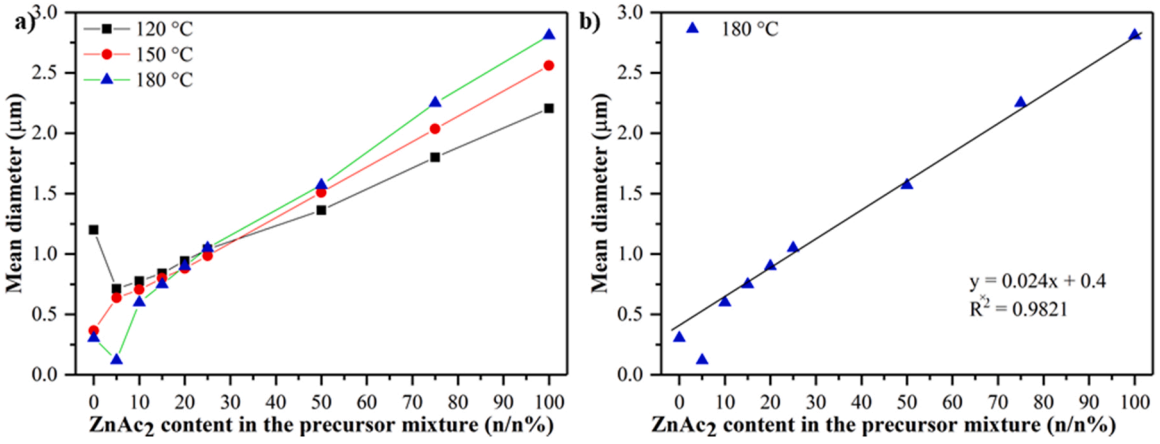

Fig. 8. Mean diameters determined from the SEM micrographs as a function of $ZnAc_2$ content of the precursor mixture for the three synthesis temperatures (a) and a linear equation fit for the 180 °C sample series (b).

acetylacetone. In the region where the $ZnAc_2$ content is 20–25 m/m% these effects are more balanced. Even though both chemicals act as chelating agents, due to the polarity of acetic acid it also has mineral acid characteristics, which in turn prompts a stronger interaction with DEA. To summarize the aforementioned observations, we can conclude that DEA is the agent which plays the key role in the formation of spherical morphology. The polarity of the anion that is released from the precursor determines the actual size of the ZnO agglomerations.

The specific surface area measurements were carried out for the 150 °C series and the pure precursor samples. The specific surface area (S_A) of the samples can be calculated based on the diameter and density of ZnO [43]. Based on the equation, the S_A of the spheres should change inverse with the diameter and canonically with the acetate precursor concentration in the 0.4–8.9 m^2/g range. However, based on the BET measurements (Fig. 9a.), the S_A values are a magnitude higher than expected. The model is further contradicted by the samples synthesized at different temperatures, where the difference is even more prominent. Thus, another approach is required to examine this anomalous change in the S_A. For this purpose, Eq. (5) was reversed to estimate mean diameters (d_{BET}) corresponding to measured S_As. The results were represented together with the data obtained from the W-H analysis in Fig. 9b.

$$S_A = \frac{6}{d_{BET} \times \rho} \times 10^{-6} \quad (5)$$

where d_{BET} is the diameter of spheres and ρ is the density of ZnO (5.606 g/cm^3).

Previously, the change in mean crystallite size is small (< 2 nm) for the samples synthesized from precursor mixtures. Yet this change is well-reflected for d_{BET} and shows a linear decreasing trend. Although this relation yields correct results, it should be applied cautiously, because an inverse multiplicative or a linear relationship between the diameter of spheres and S_A would produce a very similar variance in this range.

The result may further be obscured by the precision of the BET method, so these S_A estimates should be considered as approximate values. The observed linear trend between the particle size (both **d_{BET} and $d_{W\text{-}H}$**) and $ZnAc_2$ content (Fig. 9b.) is clearly indicative of the following:

i) it suggests that the crystallites were not closely packed in the spheres, resulting in a higher surface area;
ii) it reinforces that the crystallization and the agglomeration of crystallites to spheres are clearly separate processes;
iii) the synthesis procedure offers a possibility to control morphological aspects (secondary and primary particle size) and the structure relatively independent of each other.

The data so far is sufficient to conceptualize how can the spherical morphology be controlled, which is shown in Fig. 10. At first, the crystallization of ZnO particles starts by the hydrolysis of the precursor-DEA complexes. During formation the surface of the crystallite could be saturated with various hydrolysis by-products (acetate and

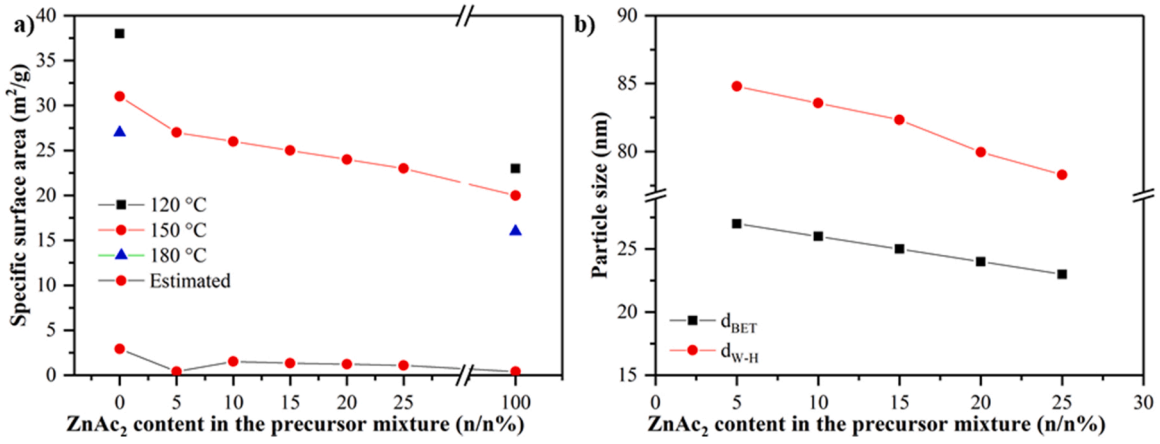

Fig. 9. Specific surface area calculations: d_{BET} is the estimated mean particle size corresponding to specific surface area measured with BET method, respectively $d_{W\text{-}H}$ average crystallite size by Williamson-Hall method.

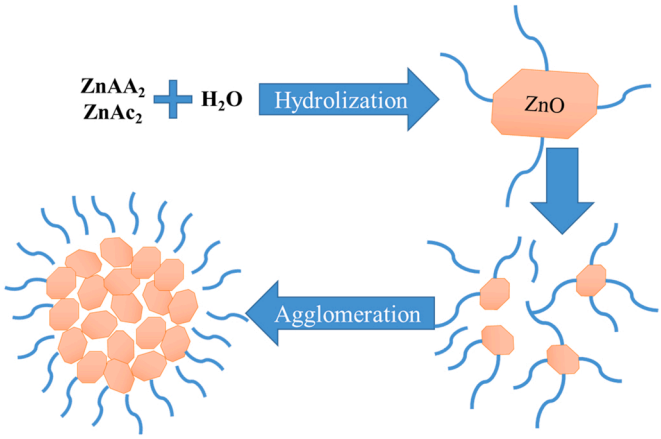

Fig. 10. Proposed mechanism of the formation of ZnO spheres.

acetylacetonate anions, respective DEA and water) due to noncovalent interactions. This could limit the crystal growth resulting in small size of the crystals. The adsorbed DEA on the surface of the particles could facilitate the aggregation of the particles through hydrogen bonding. The high surface energy due to the small size of the particles could also contribute the tendency to form spherical aggregates and reduce the surface area.

The results of the IR measurements are shown in Fig. 11. First, the main region of ZnO vibrations (Zn-O stretching, Zn-O-Zn bending) were identified in the range of 390–540 cm^{-1}. The bands corresponding to stretching vibrations of O-H of adsorbed water are situated around 3434 cm^{-1}. The spectrum contains bands with low intensity associated with organic compounds, but surprisingly their ratio with the Zn-O stretching vibrations is very low compared to the data available from the literature [36]. Most probably this is because the addition of water in our reaction mixture prevented the chemisorption of organic compounds on the surface, indicating the high purity of the product. The identified by-products with their corresponding wavenumbers were the following: N–H (3250 and 910 cm^{-1}), C–N (1270 cm^{-1}), C═O (1616 and 1396 cm^{-1}), C–O (1065 cm^{-1}), C–H and CH_2 (2973, 2925 and 2856 cm^{-1}). Due to the low intensity of these impurities, there is no observable difference between the various ZnO spheres from this point of view.

Optical proprieties of the samples were investigated with diffuse reflectance spectroscopy. The DR data were further processed using the Kubelka-Munk transformation and a derivative method to calculate the optical band-gap energy. In Fig. 11. it can be observed that no significant change occurs in the spectra of the different samples. The band-gap values decreased according to the acetate concentration, but from the perspective of the applied methods, this change is insignificant (3.12–3.19 eV). These results imply that the synthesized semiconductors can have notable photocatalytic activity under UV-A irradiation.

3.3. Photocatalytic activity

The photocatalytic activity measurements were carried out for those ZnO samples that clearly had spherical morphology. Phenol was used as model pollutants under UV-A irradiation, and the results were summarized in Fig. 12. for some representative samples.

As expected, the adsorption of the model compounds in the dark was less than 1% for all of the samples, because phenol does not adsorb well on pure ZnO in general. For the phenol degradation curves a linear model could be fitted the best (R^2 >98%). As the photocatalytic degradation progresses and the C/C_0 falls below 0.04, the behavior of the curves turns from linear to asymptotic. Even though the concentration change is very close to linear, which suggest a zeroth order kinetics, the photocatalytic degradation of phenol should be considered pseudo first order, because the degradation pathway of phenol involves various intermediates (hydroquinone, resorcinol, hydroxyquinol, catechol, etc.) [44]. These intermediates were also identified in our case, also their complete degradation takes place after 3 h (Fig. S2.). The various structural and morphological differences of the samples result in a wide range of degradation efficiencies, ranging from 5% to 99%. To clarify the causal relationship between the material proprieties and photocatalytic activity, a separate section will be dedicated for this purpose (Section 3.5).

3.4. Catalyst re-use

Unfortunately, ZnO is more prone to photocorrosion than other photocatalysts such as TiO_2 [45]. This is due to the reactivity of surface Zn ions towards the generated hydroxyl groups that results in the formation of zinc hydroxide. Ultimately, this changes the structure of the catalyst's surface and causes its deactivation; however, photostability is a main requirement of any catalyst for practical applications. The best performing NS180 was tested to investigate how the re-use of the catalysts affects their morphology and photocatalytic efficiency. During the re-use experiments, after 1 h of degradation the catalyst was separated by centrifugation and introduced in a freshly made phenol solution and the degradation experiment was repeated. In Fig. 14. it can be seen that the catalytic activity is indeed declining with each cycle. The highest decline can be observed after the second re-use, but after that the rate of decline is less and less, showing an asymptotic behavior. The X-ray diffractogram of the reused sample (Fig. S3.) show no structural modification or impurity phases, which indicate a good stability of the

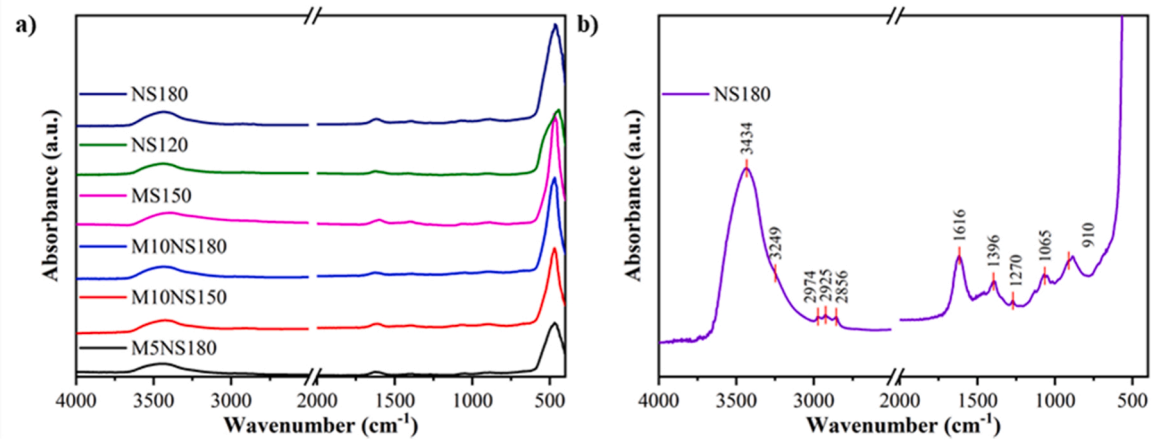

Fig. 11. FT-IR spectra of the investigated photocatalysts: (b) is a magnified (a).

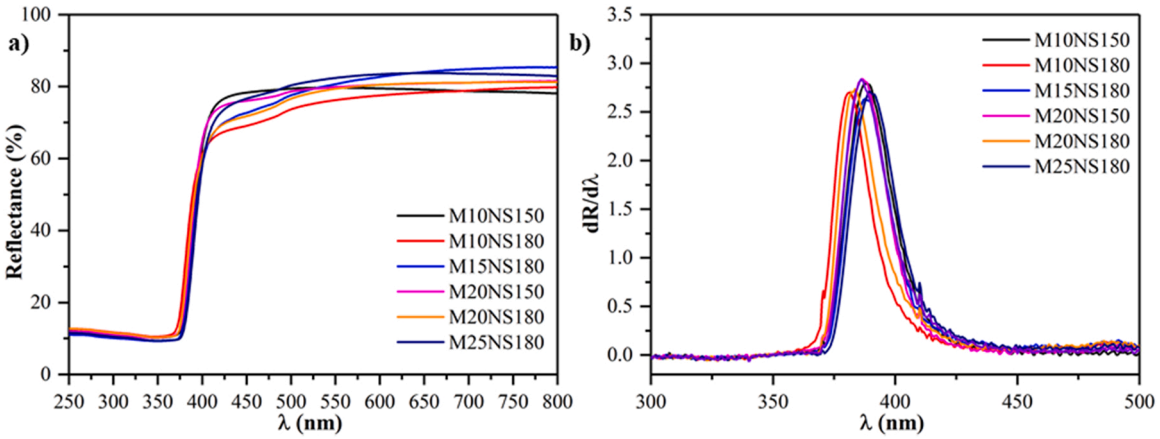

Fig. 12. DR spectra (a) and their respective first-order derivative spectra(b) of some of the ZnO semiconductors.

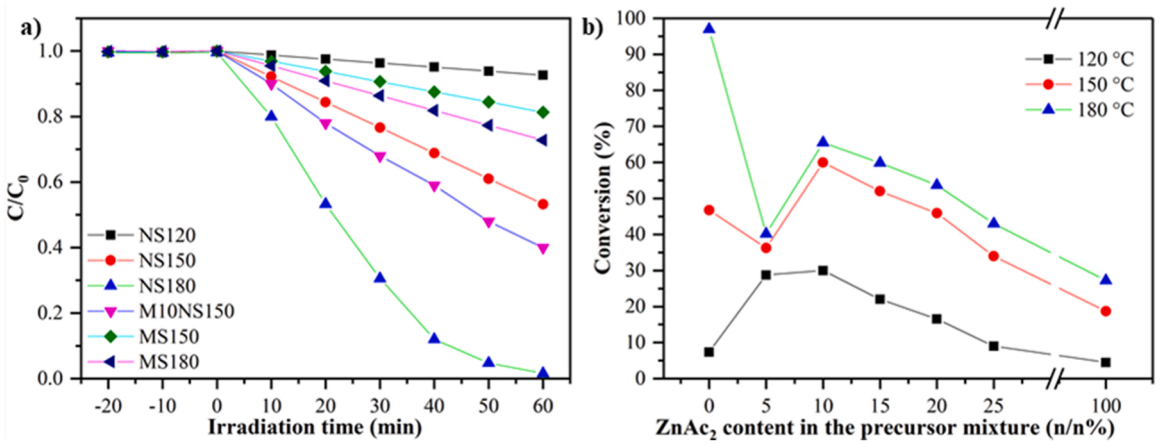

Fig. 13. Photocatalytic activity of the investigated photocatalysts for phenol degradation under UV light irradiation (a) and the correlation between the precursor ratio used during the synthesis and the observed photocatalytic activity.

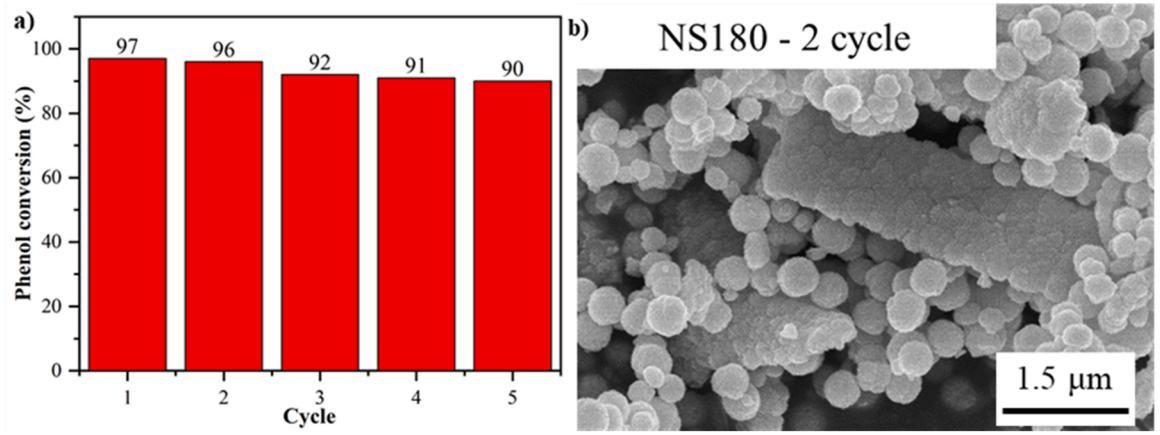

Fig. 14. Catalyst re-use for NS180: phenol conversion measured for 5 cycles of reuse of the catalyst (a) and a SEM micrograph of the dried ZnO sample after the second cycle (b).

catalyst. The cause of the decreasing activity could be explained by examining the SEM micrographs of the re-used dried catalyst. It was found that aggregates were formed from the smaller spheres, as the photocorroded ZnO surfaces of two spheres came into contact. The reason is that they could stick to each other easier in the suspension as the formed zinc hydroxide regions on the surface of the particle, exhibit higher hydrogen bonding interaction.

3.5. Further characterization of the photocatalysts

An actual full explanation for the photocatalytic activity is a delicate subject as there is no known perfect "recipe", because of the large number of parameters that can influence it. None of the observed trends can fully explain the variation in the photocatalytic activity and that why does it change from sample to sample. The following observations

were considered from the previous sections:

- DR and FT-IR measurements do not show conclusive differences between the samples.
- The crystallite size better correlate with the specific surface area of the samples, than the diameter of spheres.
- Among the structural features, the (002) and (100) crystallographic planes' diffraction intensity ratio ($r_{(002)/(100)}$) is the only one that has an anomalous effect on the photocatalytic activity.

The turnover frequency for the photocatalytic tests was calculated according to Eq. (5) [46]for NS, MS samples synthesized at 120, 150, 180 °C and MNS samples at 150 °C.

$$TOF = \frac{\Delta C}{S_A \times C_{cat}} \quad (6)$$

where TOF is turnover frequency in nmol/$m^{2\cdot h}$, ΔC is the concentration change of phenol in hour, S_A is specific surface area of the sample, C_{cat} is catalyst concentration (1 $g\cdot L^{-1}$). Based on Fig. 15b. and d. much higher photocatalytic activity can be achieved with 150 and 180 °C synthesis temperature and $r_{(002)/(100)}$. These two parameters show very similar trend, which also makes probable, that they are closely related. The trend in $r_{(002)/(100)}$ shows that (002) crystallographic planes during formation of the ZnO crystal, could be more favored at higher temperatures (>150 °C). This tendency of the growth of the crystal could also increase the defects specific to that crystallographic planes, which are more beneficial to activity. Yet, a bigger crystal could also better maintain the resultant electron-hole pair, resulted from the excitation of the catalyst. Both reflect the change in the activity, the difference in crystallite size is much sensible and correlate much simpler with the specific surface, nonetheless.

The calculated turnover frequency combines the specific surface area and the observed photocatalytic activity, which represented (Fig. 15d.) in function of the composition of the precursor mixture is very similar to the graph with conversion in function of composition (Fig. 13b.). In the present work, we propose for the present case that structural features ($r_{(002)/(100)}$, crystallite size) are predominantly responsible for the photocatalytic activity. The spherical morphology forms secondarily from the agglomeration of the crystallites. This process does not modify (or the modification is very similar for all cases) the overall activity of primary particles. The dependence of the photocatalytic activity of ZnO particles with various (100) and (002) intensity ratios has been reported a few times in the literature [47–49]. The change in activity was attributed to the intrinsic high energy of facets along (002) planes, which could promote the adsorption of OH^- and O_2 [50]. These are the main reactants for the generation of the reactive species, which are required for the degradation of organic pollutants. The increase of the ratio of these crystallographic planes not always leads to higher activity. In our previous study it was shown that an optimum value is in the range of 0.75–0.80 [51]. If we assume that the reactants (OH^-, O_2) are predominantly adsorbed on the (002) facets and the charge separations predominantly occur in other geometrical regions of the crystal, then a low proportion of this facet does not supply enough reactants to fuel the photocatalytic process. Likewise, the high ratio could supersede the regions responsible for the generation of electron-hole pairs.

4. Conclusions

ZnO photocatalysts with spherical morphology were synthesized via a solvothermal method applying DEA as morphology controlling agents. By using two precursors, that is, zinc-acetate dihydrate and zinc-acetylacetonate monohydrate, spheres with two different scales of

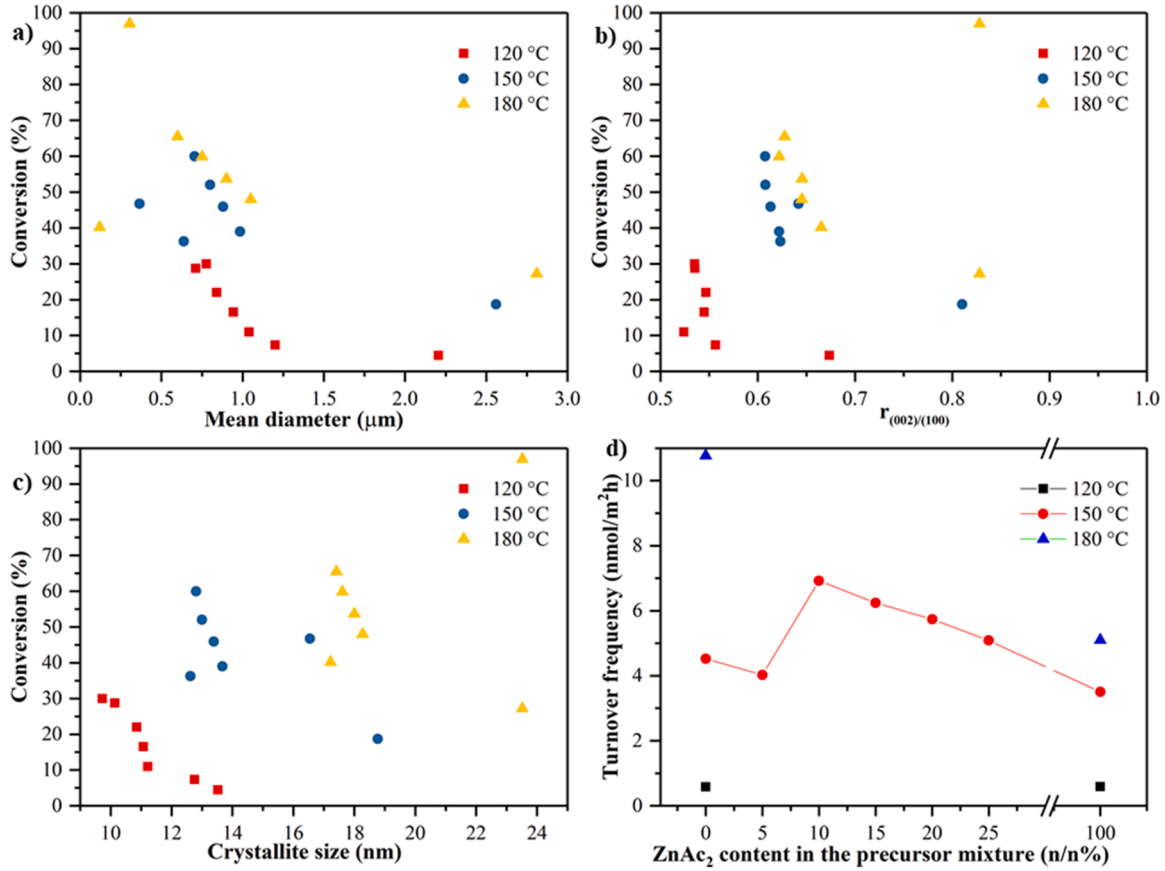

Fig. 15. Material properties relation with the photocatalytic activity.

mean diameters were obtained (305 nm and 2.813 μm, respectively). First, the water content of the solvent was investigated to find the optimal synthesis parameters to prepare photocatalytically active semiconductors while maintaining the morphology as well. 99–1% ethanol/water ratio was found to be the optimal composition, as high ethanol content is necessary for the spheres to be formed and 1% water is essential for high crystallinity and photocatalytic activity of the ZnO samples.

Two other parameters of the synthesis method were examined to influence the activity and the size of the particles: temperature of the solvothermal treatment (120, 150, 180 °C), and the ratio of the two precursors (5:95, 10:90, 15:85, 20:80, 25:75, 50:50, 75:25). Based on the SEM measurements, the average diameter of the spheres changed linearly with the increase of concentration of the acetate precursor, while the pure (i.e., not mixed) precursor show exponential trend with the temperature. The XRD patterns were used to determine the crystallite size of the samples using the three different approaches. Out of them the W-H method proved to be the most accurate, as it was confirmed by TEM measurements. The crystallite size of the mixed samples was always lower with ~30% than that of the pure precursors, and it changes according to the precursor composition. With the solvothermal temperature the crystallite size can be increased, while retaining the morphology. The specific surface areas were between 16 and 38 $m^2 \bullet g^{-1}$, which was not in accordance with the estimated values that were calculated based on the average diameters. From this it was revealed that the specific surface area is a function of the crystallite size and depends on the composition of precursor. The FT-IR measurements confirmed the high purity of the samples.

To summarize the morphological observations, with the presented synthesis method the size of the ZnO spheres can be accurately controlled in the continuous range of 120–2800 nm with similar high specific surface area. The formation of the spheres was found to be a two-stage process: it starts with the crystallization of ZnO particles in the range of 9–24 nm, then spheres were formed via agglomeration according to the precursor composition.

The photocatalytic degradation of phenol was investigated, and it was concluded that the ZnO samples with different precursor ratios exhibit activity proportionally to the samples synthesized from pure precursors. Even though the data was insufficient to mathematically correlate to the photocatalytic activity, it was found that the increased ratio of the (200) and (100) crystallographic planes greatly improve it.

CRediT authorship contribution statement

Zoltán Kovács: Investigation, Writing – original draft, Conceptualization. **Csanád Molnár:** Investigation. **Tamás Gyulavári:** Investigation. **Klára Magyari:** Investigation. **Zsejke-Réka Tóth:** Investigation. **Lucian Baia:** Writing – review & editing. **Zsolt Pap:** Supervision, Writing – original draft. **Klára Hernádi:** Funding acquisition, Writing – review & editing.

Declaration of Competing Interest

The authors declare that they have no known competing financial interests or personal relationships that could have appeared to influence the work reported in this paper.

Acknowledgments

This study was financed by the NKFI-K-124212 project. Z. Kovács is grateful for the financial support of the GINOP-2.3.2-15-2016-00013, NTP-NFTÖ-21-B-0330 and the NKFI-TNN-16-123631 projects. Zs. Pap and K. Magyari acknowledges the Bolyai János scholarship provided by the Hungarian Academy of Sciences.

Appendix A. Supporting information

Supplementary data associated with this article can be found in the online version at doi:10.1016/j.cattod.2022.03.004.

References

[1] B.M. Rajbongshi, S.K. Samdarshi, Cobalt-doped zincblende-wurtzite mixed-phase ZnO photocatalyst nanoparticles with high activity in visible spectrum, Appl. Catal. B Environ. 144 (2014) 435–441, https://doi.org/10.1016/j.apcatb.2013.07.048.
[2] W. Yu, J. Zhang, T. Peng, New insight into the enhanced photocatalytic activity of N-, C- and S-doped ZnO photocatalysts, Appl. Catal. B Environ. 181 (2016) 220–227, https://doi.org/10.1016/j.apcatb.2015.07.031.
[3] J. Mishra, M. Jha, N. Kaur, A.K. Ganguli, Room temperature synthesis of urea based imidazole functionalised ZnO nanorods and their photocatalytic application, Mater. Res. Bull. 102 (2018) 311–318, https://doi.org/10.1016/j.materresbull.2018.02.045.
[4] L. Pan, G.Q. Shen, J.W. Zhang, X.C. Wei, L. Wang, J.J. Zou, X. Zhang, TiO2-ZnO composite sphere decorated with ZnO clusters for effective charge isolation in photocatalysis, Ind. Eng. Chem. Res. 54 (2015) 7226–7232, https://doi.org/10.1021/acs.iecr.5b01471.
[5] H. Wang, D. Peng, T. Chen, Y. Chang, S. Dong, A novel photocatalyst AgBr/ZnO/RGO with high visible light photocatalytic activity, Ceram. Int. 42 (2016) 4406–4412, https://doi.org/10.1016/j.ceramint.2015.11.124.
[6] C. Yu, K. Yang, Q. Shu, J.C. Yu, F. Cao, X. Li, Preparation of WO3/ZnO composite photocatalyst and its photocatalytic performance, Chin. J. Catal. 32 (2011) 555–565, https://doi.org/10.1016/s1872-2067(10)60212-4.
[7] Z. Lv, Q. Zhong, M. Ou, Utilizing peroxide as precursor for the synthesis of CeO 2 /ZnO composite oxide with enhanced photocatalytic activity, Appl. Surf. Sci. 376 (2016) 91–96, https://doi.org/10.1016/j.apsusc.2016.01.280.
[8] Y. Geng, N. Li, J. Ma, Z. Sun, Preparation, characterization and photocatalytic properties of BiOBr/ZnO composites, J. Energy Chem. 26 (2017) 416–421, https://doi.org/10.1016/j.jechem.2017.01.002.
[9] Y. Liu, J. Shi, Q. Peng, Y. Li, CuO quantum-dot-sensitized mesoporous ZnO for visible-light photocatalysis, Chem. - A Eur. J. 19 (2013) 4319–4326, https://doi.org/10.1002/chem.201203316.
[10] W. Kang, X. Jimeng, W. Xitao, The effects of ZnO morphology on photocatalytic efficiency of ZnO/RGO nanocomposites, Appl. Surf. Sci. 360 (2016) 270–275, https://doi.org/10.1016/j.apsusc.2015.10.190.
[11] M.J. Sampaio, A. Benyounes, P. Serp, J.L. Faria, C.G. Silva, Photocatalytic synthesis of vanillin using N-doped carbon nanotubes/ZnO catalysts under UV-LED irradiation, Appl. Catal. A Gen. 551 (2018) 71–78, https://doi.org/10.1016/j.apcata.2017.12.002.
[12] V. Vaiano, C.A. Jaramillo-Paez, M. Matarangolo, J.A. Navío, M. del Carmen Hidalgo, UV and visible-light driven photocatalytic removal of caffeine using ZnO modified with different noble metals (Pt, Ag and Au), Mater. Res. Bull. 112 (2019) 251–260, https://doi.org/10.1016/j.materresbull.2018.12.034.
[13] A. Das, N. S.K, R.G. Nair, Influence of surface morphology on photocatalytic performance of zinc oxide: A review, Nano-Struct. Nano-Objects 19 (2019), 100353, https://doi.org/10.1016/j.nanoso.2019.100353.
[14] H. Sun, Y. Yu, J. Luo, M. Ahmad, J. Zhu, Morphology-controlled synthesis of ZnO 3D hierarchical structures and their photocatalytic performance, CrystEngComm 14 (2012) 8626–8632, https://doi.org/10.1039/c2ce26157j.
[15] L. Zhang, L. Yin, C. Wang, N. Lun, Y. Qi, Sol-gel growth of hexagonal faceted ZnO prism quantum dots with polar surfaces for enhanced photocatalytic activity, ACS Appl. Mater. Interfaces 2 (2010) 1769–1773, https://doi.org/10.1021/am100274d.
[16] S. Mukhopadhyay, P.P. Das, S. Maity, P. Ghosh, P.S. Devi, Solution grown ZnO rods: synthesis, characterization and defect mediated photocatalytic activity, Appl. Catal. B Environ. 165 (2015) 128–138, https://doi.org/10.1016/j.apcatb.2014.09.045.
[17] F. Lu, W. Cai, Y. Zhang, ZnO hierarchical micro/nanoarchitectures: Solvothermal synthesis and structurally enhanced photocatalytic performance, Adv. Funct. Mater. 18 (2008) 1047–1056, https://doi.org/10.1002/adfm.200700973.
[18] X.W. Wang, L. Zhou, F. Li, ZnO disks loaded with reduced graphene oxide for the photodegradation of methylene blue, N. Carbon Mater. 28 (2013) 408–413, https://doi.org/10.1016/S1872-5805(13)60090-6.
[19] Y.K. Mishra, G. Modi, V. Cretu, V. Postica, O. Lupan, T. Reimer, I. Paulowicz, V. Hrkac, W. Benecke, L. Kienle, R. Adelung, Direct growth of freestanding ZnO tetrapod networks for multifunctional applications in photocatalysis, UV photodetection, and gas sensing, ACS Appl. Mater. Interfaces 7 (2015) 14303–14316, https://doi.org/10.1021/acsami.5b02816.
[20] Z. Deng, M. Chen, A. Gu, L. Wu, A facile method to fabricate ZnO hollow spheres and their photocatalytic property, J. Phys. Chem. B. 112 (2008) 16–22, https://doi.org/10.1021/jp077662w.
[21] H. Lv, G. Ji, Z. Yang, Y. Liu, X. Zhang, W. Liu, H. Zhang, Enhancement photocatalytic activity of the graphite-like C3N4 coated hollow pencil-like ZnO, J. Colloid Interface Sci. 450 (2015) 381–387, https://doi.org/10.1016/j.jcis.2015.03.038.
[22] Q.P. Luo, X.Y. Yu, B.X. Lei, H.Y. Chen, D. Bin Kuang, C.Y. Su, Reduced graphene oxide-hierarchical ZnO hollow sphere composites with enhanced photocurrent and photocatalytic activity, J. Phys. Chem. C. 116 (2012) 8111–8117, https://doi.org/10.1021/jp2113329.

[23] C. Zhu, B. Lu, Q. Su, E. Xie, W. Lan, A simple method for the preparation of hollow ZnO nanospheres for use as a high performance photocatalyst, Nanoscale 4 (2012) 3060–3064, https://doi.org/10.1039/c2nr12010k.
[24] W. Chen, Q. Liu, S. Tian, X. Zhao, Exposed facet dependent stability of ZnO micro/nano crystals as a photocatalyst, Appl. Surf. Sci. 470 (2019) 807–816, https://doi.org/10.1016/j.apsusc.2018.11.206.
[25] D. Chen, Z. Wang, T. Ren, H. Ding, W. Yao, R. Zong, Y. Zhu, Influence of defects on the photocatalytic activity of ZnO, J. Phys. Chem. C. 118 (2014) 15300–15307, https://doi.org/10.1021/jp5033349.
[26] X. Pan, M.Q. Yang, Y.J. Xu, Morphology control, defect engineering and photoactivity tuning of ZnO crystals by graphene oxide-a unique 2D macromolecular surfactant, Phys. Chem. Chem. Phys. 16 (2014) 5589–5599, https://doi.org/10.1039/c3cp55038a.
[27] M. Farbod, E. Jafarpoor, Fabrication of different ZnO nanostructures and investigation of morphology dependence of their photocatalytic properties, Mater. Lett. 85 (2012) 47–49, https://doi.org/10.1016/j.matlet.2012.06.080.
[28] T.J. Liu, Q. Wang, P. Jiang, Morphology-dependent photo-catalysis of bare zinc oxide nanocrystals, RSC Adv. 3 (2013) 12662–12670, https://doi.org/10.1039/c3ra41399c.
[29] S. Del Gobbo, J. Poolwong, V. D'Elia, In-suspension growth of ZnO nanorods with tunable length and diameter using polymorphic seeds, Cryst. Growth Des. 19 (2019) 6792–6800, https://doi.org/10.1021/acs.cgd.9b01226.
[30] A. Šarić, I. Despotović, G. Štefanić, G. Dražić, The influence of ethanolamines on the solvothermal synthesis of zinc oxide: a combined experimental and theoretical study, ChemistrySelect 2 (2017) 10038–10049, https://doi.org/10.1002/slct.201701692.
[31] A. Gómez-Núñez, S. Alonso-Gil, C. López, P. Roura-Grabulosa, A. Vilà, From ethanolamine precursor towards ZnO—how N is released from the experimental and theoretical points of view, Nanomaterials 9 (2019).
[32] V. Mote, Y. Purushotham, B. Dole, Williamson-Hall analysis in estimation of lattice strain in nanometer-sized ZnO particles, J. Theor. Appl. Phys. 6 (2012) 2–9, https://doi.org/10.1186/2251-7235-6-6.
[33] A. Khorsand Zak, W.H. Abd. Majid, M.E. Abrishami, R. Yousefi, X-ray analysis of ZnO nanoparticles by Williamson-Hall and size-strain plot methods, Solid State Sci. 13 (2011) 251–256, https://doi.org/10.1016/j.solidstatesciences.2010.11.024.
[34] R. Yogamalar, R. Srinivasan, A. Vinu, K. Ariga, A.C. Bose, X-ray peak broadening analysis in ZnO nanoparticles, Solid State Commun. 149 (2009) 1919–1923, https://doi.org/10.1016/j.ssc.2009.07.043.
[35] X. Wang, Q. Zhang, Q. Wan, G. Dai, C. Zhou, B. Zou, Controllable ZnO architectures by ethanolamine-assisted hydrothermal reaction for enhanced photocatalytic activity, J. Phys. Chem. C 115 (2011) 2769–2775, https://doi.org/10.1021/jp1096822.
[36] A. Šarić, G. Štefanić, G. Dražić, M. Gotić, Solvothermal synthesis of zinc oxide microspheres, J. Alloy. Compd. 652 (2015) 91–99, https://doi.org/10.1016/j.jallcom.2015.08.200.
[37] Y. Inubushi, R. Takami, M. Iwasaki, H. Tada, S. Ito, Mechanism of formation of nanocrystalline ZnO particles through the reaction of [Zn(acac)2] with NaOH in EtOH, J. Colloid Interface Sci. 200 (1998) 220–227, https://doi.org/10.1006/jcis.1997.5354.
[38] J.E. Rodríguez-Paéz, A.C. Caballero, M. Villegas, C. Moure, P. Durán, J. F. Fernández, Controlled precipitation methods: formation mechanism of ZnO nanoparticles, J. Eur. Ceram. Soc. 21 (2001) 925–930, https://doi.org/10.1016/S0955-2219(00)00283-1.
[39] S.C. Singh, Effect of oxygen injection on the size and compositional evolution of ZnO/Zn(OH)2 nanocomposite synthesized by pulsed laser ablation in distilled water, J. Nanopart. Res. 13 (2011) 4143–4152, https://doi.org/10.1007/s11051-011-0359-2.
[40] P. Bindu, S. Thomas, Estimation of lattice strain in ZnO nanoparticles: X-ray peak profile analysis, J. Theor. Appl. Phys. 8 (2014) 123–134, https://doi.org/10.1007/s40094-014-0141-9.
[41] C.F. Holder, R.E. Schaak, Tutorial on powder X-ray diffraction for characterizing nanoscale materials, ACS Nano 13 (2019) 7359–7365, https://doi.org/10.1021/acsnano.9b05157.
[42] M.A.R. Miranda, J.M. Sasaki, The limit of application of the Scherrer equation, Acta Crystallogr. Sect. A 74 (2018) 54–65, https://doi.org/10.1107/S2053273317014929.
[43] B.Y. Shekunov, P. Chattopadhyay, H.H.Y. Tong, A.H.L. Chow, Particle size analysis in pharmaceutics: principles, methods and applications, Pharm. Res. 24 (2007) 203–227, https://doi.org/10.1007/s11095-006-9146-7.
[44] A.M. Al-Hamdi, M. Sillanpää, J. Dutta, Intermediate formation during photodegradation of phenol using lanthanum doped tin dioxide nanoparticles, Res. Chem. Intermed. 42 (2016) 3055–3069, https://doi.org/10.1007/s11164-015-2197-9.
[45] S. Ahmed, M.G. Rasul, W.N. Martens, R. Brown, M.A. Hashib, Heterogeneous photocatalytic degradation of phenols in wastewater: a review on current status and developments, Desalination 261 (2010) 3–18, https://doi.org/10.1016/j.desal.2010.04.062.
[46] I.E. Wachs, S.P. Phivilay, C.A. Roberts, Reporting of reactivity for heterogeneous photocatalysis, ACS Catal. 3 (2013) 2606–2611, https://doi.org/10.1021/cs4005979.
[47] C.A. Jaramillo-Páez, J.A. Navío, M.C. Hidalgo, M. Macías, ZnO and Pt-ZnO photocatalysts: characterization and photocatalytic activity assessing by means of three substrates, Catal. Today 313 (2018) 12–19, https://doi.org/10.1016/j.cattod.2017.12.009.
[48] J. Gupta, K.C. Barick, D. Bahadur, Defect mediated photocatalytic activity in shape-controlled ZnO nanostructures, J. Alloy. Compd. 509 (2011) 6725–6730, https://doi.org/10.1016/j.jallcom.2011.03.157.
[49] C. Jaramillo-Páez, J.A. Navío, M.C. Hidalgo, M. Macías, High UV-photocatalytic activity of ZnO and Ag/ZnO synthesized by a facile method, Catal. Today 284 (2017) 121–128, https://doi.org/10.1016/j.cattod.2016.11.021.
[50] E.-S. Jang, J. Won, S.-J. Hwang, J.-H. Choy, Fine tuning of the face orientation of ZnO crystals to optimize their photocatalytic activity, Adv. Mater. 18 (2006) 3309–3312, https://doi.org/10.1002/adma.200601455.
[51] Z. Kovács, C. Molnár, U.L. Štangar, V.M. Cristea, Z. Pap, K. Hernadi, L. Baia, Article optimization method of the solvothermal parameters using box–behnken experimental design—the case study of zno structural and catalytic tailoring, Nanomaterials 11 (2021), https://doi.org/10.3390/nano11051334.